



Article

# Object-Oriented Landslide Mapping Using ZY-3 Satellite Imagery, Random Forest and Mathematical Morphology, for the Three-Gorges Reservoir, China

Tao Chen <sup>1,2,\*</sup>, John C. Trinder <sup>2</sup> and Ruiqing Niu <sup>1</sup>

<sup>1</sup> Institute of Geophysics and Geomatics, China University of Geosciences, Wuhan 430074, China; rqniu@163.com

<sup>2</sup> Surveying and Geospatial Engineering, School of Civil and Environmental Engineering, The University of New South Wales, Sydney, NSW 2052, Australia; j.trinder@unsw.edu.au

\* Correspondence: taochen@cug.edu.cn; Tel.: +86-27-6788-3251

Academic Editors: Zhong Lu, Chaoying Zhao and Prasad S. Thenkabail

Received: 9 January 2017; Accepted: 29 March 2017; Published: 31 March 2017

**Abstract:** Landslide mapping (LM) has recently become an important research topic in remote sensing and geohazards. The area near the Three Gorges Reservoir (TGR) along the Yangtze River in China is one of the most landslide-prone regions in the world, and the area has suffered widespread and significant landslide events in recent years. In our study, an object-oriented landslide mapping (OOLM) framework was proposed for reliable and accurate LM from ‘ZY-3’ high spatial resolution (HSR) satellite images. The framework was based on random forests (RF) and mathematical morphology (MM). RF was first applied as an object feature information reduction tool to identify the significant features for describing landslides, and it was then combined with MM to map the landslides. Three object-feature domains were extracted from the ‘ZY-3’ HSR data: layer information, texture, and geometric features. A total group of 124 features and 24 landslides were used as inputs to determine the landslide boundaries and evaluate the landslide classification accuracy. The results showed that: (1) the feature selection (FS) method had a positive influence on effective landslide mapping; (2) by dividing the data into two sets, training sets which consisted of 20% of the landslide objects ( $O_{LS}$ ) and non-landslide objects ( $O_{NLS}$ ), and test sets which consisted of the remaining 80% of the  $O_{LS}$  and  $O_{NLS}$ , the selected feature subsets were combined for training to obtain an overall classification accuracy of  $93.3\% \pm 0.12\%$  of the test sets; (3) four MM operations based on closing and opening were used to improve the performance of the RF classification. Seven accuracy evaluation indices were used to compare the accuracies of these landslide mapping methods. Finally, the landslide inventory maps were obtained. Based on its efficiency and accuracy, the proposed approach can be employed for rapid response to natural hazards in the Three Gorges area.

**Keywords:** Landslide mapping (LM); Random forest (RF); ZY-3; The Three Gorges; Feature selection (FS)

## 1. Introduction

The socio-economic stability of the area near the Three Gorges Reservoir (TGR) along the Yangtze River in China is under serious threat caused by many active small and large landslides, which are major geological hazards in the region. More than 3800 landslides have been reported [1], progressively causing injuries and casualties to individuals as well as significant economic and environmental consequences [2–5]. Though considerable attention has been paid to landslide mapping (LM) over the past few decades, mapping landslides reliably and accurately for practical engineering applications has proved to be difficult [6–9]. Traditional field surveys are often time-consuming, labor-intensive, and costly, even though they can achieve reliable results [10].

Nowadays, the availability of high spatial resolution (HSR) remote sensing satellite images have enabled more reliable mapping of landslides more rapidly than ever before [2,11,12]. There has been considerable research on LM based on HSR data, such as IKONOS [13], pan-sharpened Quickbird [14], pan-sharpened Advanced Land Observing Satellite (ALOS) [15], and airborne Light Detection And Ranging (LIDAR) [16]. For the monitoring of slow-moving landslides and LM in cloudy areas, Synthetic Aperture Radar (SAR) images and Interferometric SAR (InSAR) technology have been widely used because of their advantages over optical images [17,18]. Although there has been considerable research on LM based on HSR satellite images, until now the use of the Chinese 'ZY-3' satellite data for LM in TGR has not been reported in academic publications.

Current methods for LM can be grouped into two broad categories of pixel based (PB) and object-oriented (OO) approaches. The most commonly used PB methods for LM are based on change detection (CD) because of its simplicity and applicability [19]. Although it has been applied for different HSR satellite images, the limitation of this method is the diversity of the landslide components which have affected the accuracy of the detected changes [20]. Other PB methods such as image matching techniques [21] and machine learning [22] have also achieved satisfactory LM results.

Object-oriented approaches, for which the units are image objects, consisting of pixels with similar spectral signatures, have become widely used for many geoscience related research projects in order to exploit geometric and contextual image information from multi-source data, which are often unavailable for the traditional PB methods [23,24]. Some researchers have proved that using an OO approach can lead to feasible results by combining CD [25], segmentation optimization methods [26], and spatiotemporal analysis [27,28]. However, the identification of landslide boundaries and the context characteristics of neighborhood objects have not been adequately defined to produce a reliable LM.

Landslides, which can be briefly described as the movement of rock, soil, or debris down a slope, are complex systems, and are expected to occur under circumstances similar to those that have led to past slope failures [29]. Effective object-oriented landslide mapping (OOLM) requires the definition of object-features from remote sensing and thematic data, such as image band information, texture, and geometric features ranging in number from several to dozens. However, there are no universal guidelines for feature selection (FS) that can influence the accuracy of OOLM. When a large number of features are available, the extraction of the appropriate features for different study areas is a complex process, while various OOLM models can also be applied.

The random forests (RF) algorithm, which can provide high classification accuracy without overfitting, is based on classification trees [30]. It has been demonstrated to be an effective tool in dealing with vagueness and uncertainty of information, and has led to excellent performance for the analyses of many complex remote sensing datasets [8,31,32].

Mathematical morphology (MM), which is based on set theory, lattice theory, topology, and random functions, is used for the processing and analysis of geometrical structures [33]. Recently, MM approaches have attracted increasing attention for the consideration of topological and geometric continuous-space concepts. For example, the researchers of [20] have increased the accuracy of LM by using MM to remove errors in detected landslide candidates.

The objective of this paper is to examine the applicability of a FS method, RF algorithm, and MM method for OOLM using 'ZY-3' HSR satellite images in the TGR, China. The proposed OOLM methodology was developed using the eCognition<sup>®</sup> software (Version 9.0.1) and R statistical programming environment. The rest of this paper is organized as follows: Section 2 describes the study area and the data used and details the framework of the OOLM; Section 3 presents the experimental results; discussions are presented in Section 4; and conclusions are given in Section 5.

## 2. Materials and Methods

### 2.1. Study Area

The study area lies in Shazhenxi Town, Hubei Province, about 70 km west of the Three Gorges Dam with an area of 38.49 km<sup>2</sup> (Figure 1), located between latitudes of 31.011°N and 31.049°N, and longitudes between 110.313°E and 110.514°E, with elevations above sea level ranging from 157 m to 919 m. The Yangtze River broadly crosses the study area in a WNW–ESE direction. The climate in the area is typically subtropical, with hot and humid summers but cold and dry winters, while heavy rainfall is mainly concentrated in spring and summer, with an average annual precipitation of 1100 mm. The area is located in the transitional zone between the south end of the Zigui syncline, which is oriented mainly N–S, and the Baifuping anticline, which is oriented mainly W–E. The geological base of this area is Triassic detrital rock (Shazhenxi Group) and Jurassic silt, lutite, pelitic siltstone, and sandstone (Niejashan Group). The Niukou–Xiangluping fault zone, comprising the main faults and fracture systems in the study area, crosses the Zigui basin with an orientation of NNE–SSW, leading to the formation of ‘weak’ zones that are conducive to slope instability [34].

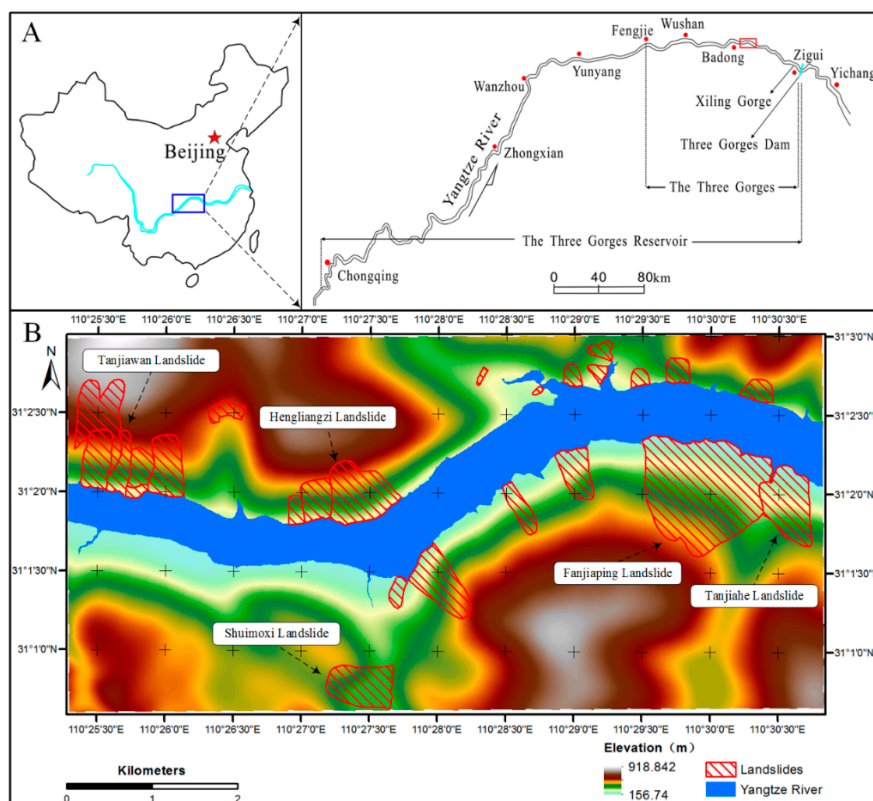


**Figure 1.** Location of the study area. (A) Site map of the Three Gorges area of the Yangtze River, China. (B) Digital elevation model (DEM) overlaid with landslides; the red hatched areas represent landslides areas.

### 2.2. Landslide Inventory, Image and Thematic Input Layers

Landslides in this study area, which mostly comprise old rock and shallow soils, were visually identified on 1:10,000-scale color aerial photographs (Figure 2). Based on a series of field surveys, and reviews of historical and bibliographical data, 24 landslides were finally mapped and subsequently digitized and rasterized in Environmental Systems Research Institute (ESRI)’s ArcGIS software (Version 10.3.0) with a grid cell size of  $5.8 \times 5.8$  m, which is the same resolution as the multispectral remote sensing data used for the study.

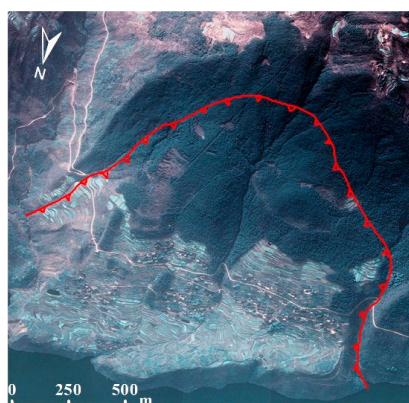


**Figure 2.** The Fanjiaping landslide identified by the aerial photographs of the landslide.

A total of eleven layers were derived as inputs from the satellite data and thematic maps (Table 1).

**Table 1.** Input layer information in this study.

Input Layer Derived from Satellite Images (Pixel Size)	Input Layer Derived from Digital Elevation Model (DEM) (Pixel Size)
<i>Panchromatic (Pan)</i> (2.1 m)	<i>Curvature</i> (5.8 m)
<i>Red</i> (5.8 m)	<i>Hillshade</i> (5.8 m)
<i>Green</i> (5.8 m)	<i>Roughness</i> (5.8 m)
<i>Blue</i> (5.8 m)	<i>Flow direction</i> (5.8 m)
<i>Near Infrared (NIR)</i> (5.8 m)	<i>Slope</i> (5.8 m)
<i>Normalized Difference Vegetation Index (NDVI)</i> (5.8 m)	

One ‘ZY-3’ HSR image with a spatial resolution of 5.8 m for the multispectral bands (Path/row, 113/132), and 2.1 m for the panchromatic band (Path/row, 113/139), acquired on 30 April 2013, was procured for this study. An Normalized Difference Vegetation Index (NDVI) map was derived from the near infrared and red bands of the ‘ZY-3’ HSR images as an additional layer. The digital elevation model (DEM) of the area with a resolution of 12.5 m was resampled to a resolution of 5.8 m to be compatible with the other data sets. Six thematic layers were derived from the DEM data as input layers in order to define the landslide features: *Curvature*, *Hillshade*, *Roughness*, *Flow direction*, and *Slope*.

### 2.3. Methodology

The OOLM framework, shown in Figure 3, consists of two steps: *image segmentation* and *landslide mapping*. For the *image segmentation*, image objects were extracted from ‘ZY-3’ HSR images and DEM data using multi-resolution segmentation (MRS). The objects were then labeled according to whether they were landslides ( $O_{LS}$ ) (which comprised more than 50% of the extracted objects), or non-landslide objects ( $O_{NLS}$ ), by combining the objects with the landslide inventory. Then a FS method based on the RF algorithm was used to reduce the feature sample dataset size, after which a 10-fold cross validation method was applied using subsets of the spatial features, where for each cross validation, 80% of the landslides were withheld for testing, to reduce potentially high spatial autocorrelation between the training and the test sets.

In the *landslide mapping* step, by combining the feature subset derived from *image segmentation*, a RF model was applied to classify the test sets into  $O_{LS}$  and  $O_{NLS}$ , and the accuracies of classification were assessed. Finally, four different MM operations, which were opening, closing, opening followed by closing, and closing followed by opening, were used to deal with the errors which were present inside and outside the extracted landslide object candidates and the classification accuracies were assessed once again.

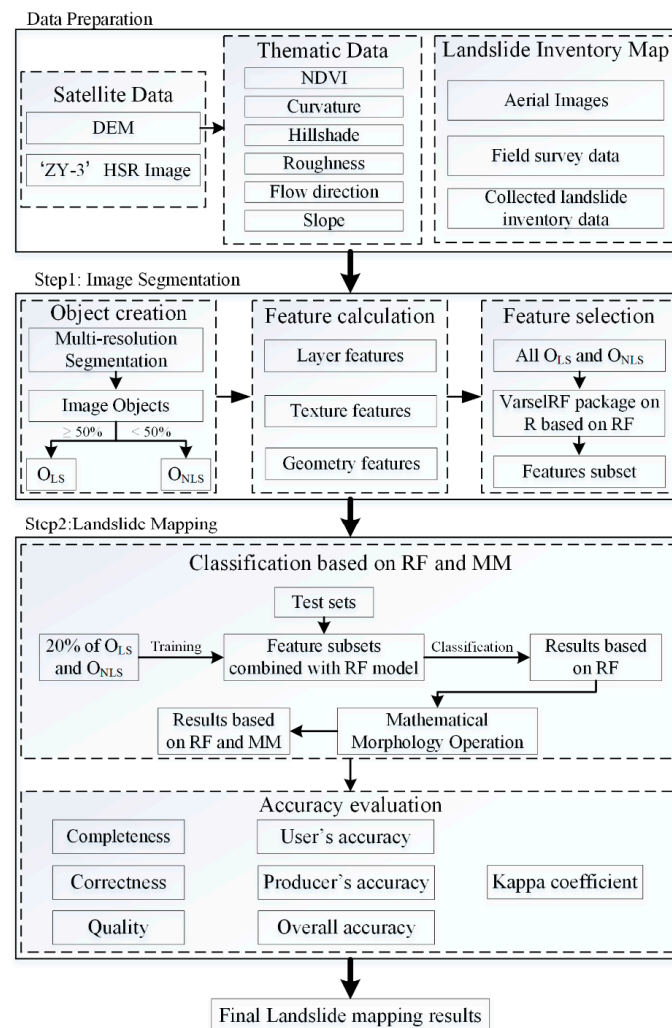


Figure 3. Flow chart of the proposed methods in this study.

### 2.3.1. Image Segmentation

For the OO method, image segmentation is the necessary and first prerequisite, because delineation qualities of the target objects such as size and shape have a direct influence on the accuracy of the subsequent image classification [35]. There are many segmentation methods, but MRS is a frequently used method in landslide studies [36] and was chosen for this study.

In the MRS procedure, three user-defined parameters are very important; scale, shape, and color. The scale parameter (SCP) is an abstract term, which determines the maximum allowed heterogeneity within the resulting image objects [37]. The color parameter (CP), which refers to the spectral homogeneity, and shape parameter (SHP), for defining the textural homogeneity of the resulting image objects, are other important parameters. They both are weighted from 0 to 1 and the sum of their weights is 1 in the eCognition<sup>®</sup> software (Version 9.0.1). The shape criterion is often divided into two groups: smoothness used to optimize image objects by regarding the smoothness of their borders; and compactness, utilized to optimize image objects with regard to their compactness.

### 2.3.2. Calculation of Object Features

In this study, three object-feature domains, which were layer, texture, and geometry, comprising a total of 124 features were extracted from the 'ZY-3' HSR data by using the eCognition<sup>®</sup> software (Version 9.0.1) (Table 2) as recommended by previous researchers [8,38].

**Table 2.** Object features used in this study.

Object-Feature Domains (No.)	Features (No.)
Layer features (57)	<i>Max</i> (11), <i>Min</i> (11), <i>Stdv</i> (standard deviation) (11), <i>Mean</i> (11), <i>Ratio</i> (11), <i>Brightness</i> (1), <i>MaxDiff</i> (1)
Texture features (60)	<i>GLCM</i> all dir. ( <i>Ent</i> (12), <i>Mean</i> (12), <i>Cor</i> (12), <i>Con</i> (12), <i>Stdv</i> (12))
Geometry features (7)	<i>Shape index</i> (1), <i>Density</i> (1), <i>Main direction</i> (1), <i>Roundness</i> (1), <i>Length-width ratio</i> (1), <i>Area</i> (1), <i>Number of Pixels</i> (1)

The *Max* and *Min* refer to the maximum and minimum pixel values, while standard deviation (*Stdv*) and *mean* refer to the standard deviation and the mean intensity values of all pixels forming an image object, respectively. The *Ratio* value is the layer mean value of an image object divided by the sum of all layer mean values. The *MaxDiff* value of each object is the absolute value of the difference of the maximum object mean value ( $\max(\bar{O}_{i(v)})$ ) and the minimum object mean value ( $\min(\bar{O}_{i(v)})$ ) in each layer, divided by the object brightness  $B$ , which was defined as the sum of the object means in the same layers ( $\bar{O}_{i(v)}$ ) divided by the number of corresponding layers ( $n_v$ ).

$$MaxDiff = \frac{|\max(\bar{O}_{i(v)}) - \min(\bar{O}_{i(v)})|}{B}, \quad (1)$$

$$B = \frac{1}{n_v} \sum_{i=1}^{n_v} (\bar{O}_{i(v)}), \quad (2)$$

The texture features used in this study were derived from the gray level co-occurrence matrix (*GLCM*), which can be used to calculate 14 textures [39]. Considering the computational efficiency and frequent reports on strong correlations among them [40], a subset of five texture measures was selected, which were *entropy* (*Ent.*), *Mean*, *correlation* (*Cor.*), *contrast* (*Con.*), and *standard deviation* (*Stdv.*). Using the eCognition® software (Version 9.0.1) [41], the *GLCM* frequencies were calculated in symmetric matrices for the four directions of neighboring pixels at 0°(N-S), 45°(NE-SW), 90°(E-W), or 135°(SW-NE), respectively, which together with the sum of the four directional *GLCMs* (*GLCM*<sub>all dir.</sub>) gave five rotation-invariant texture measures per image object for each band.

The geometric features used in this study were *Shape index*, *Density*, *Main direction*, *Roundness*, *Length-width ratio*, *Area*, and *Number of Pixels*. The *shape index* is calculated from the length of the border of each image object divided by four times the square root of its area. The *density* describes the distribution in space of the pixels of an image object. The *main direction* feature of an image object is defined as the direction of the eigenvector belonging to the larger of the two eigenvalues derived from the covariance matrix of the spatial distribution of the image object. The *roundness* is calculated from the difference of the ellipse enclosing an object and the ellipse enclosed by an object. The *length-width ratio* is the ratio of length and width of an object. The *area* is simply the number of pixels that form the image object.

### 2.3.3. Random Forests-Based Landslide Mapping (RFLM)

The RF algorithm, which was developed by [30], has been widely used in many fields of study in remote sensing and has been considered as an efficient non-parametric ensemble learning decision tree based method, because of its excellent performance for classification or regression [16,42,43]. It was selected as the landslide mapping model in this study, based on its ability in finding useful patterns in large volumes of data.

It is known that many problems can be caused by large feature sets in the process of classification, such as: low efficiency due to the numerous resources [44], loss of accuracy when the optimal number of features is significantly lower than the number of features [45], and unrelated input features, which may cause model overfitting. Therefore, eliminating redundant or correlated features in the input layers is important for improving the classification accuracy for a particular study area.

In this paper, the varSelRF package [46] implemented in the R statistical programming environment [47] was used for feature selection, which is based on the random forest (RF) algorithm [48]. A procedure which was proposed by [49] based on two RFs was applied to determine the feature subsets that were recommended for the construction of the final RF classifiers. The first RF was used to create an initial feature ranking with the numbers set to 3000, while the second RF was used to exclude the least important 20% of the features based on an iterative process with the numbers set to 1000. All  $O_{LS}$  and an equal number of randomly selected  $O_{NLS}$  were applied for feature selection. One third of them were used for the training set and the remainder as an out-of-bag (OOB) sample, were used to assess the second RF misclassification rate (OOB error). Following the method of [8], the final feature subset was selected according to the RF that produced the lowest OOB error.

### 2.3.4. Mathematical Morphology Operation

Although the RF method can achieve effective results in LM, its performance can be further improved by eliminating some errors which are present both outside and inside the landslide candidates. In order to improve the performance, two MM operations (opening and closing) and their combinations (opening followed by closing, closing followed by opening) were successively applied to the RFLM results [33]. The type of the structuring elements used in this paper was a  $1 \times 3$  array  $k$ ,  $k = \{1, 1, 1\}$ .

## 3. Results

### 3.1. Image Segmentation and Feature Selection

Although some new tools are proposed to estimate the SCP for segmentation processes [31,50], its selection still often requires an iterative trial-and-error optimization method because the segmentation quality can be visually assessed [51]. After several trial-and-error attempts to find the proper MRS parameters [52], in order to ensure that the segment boundaries of the smallest landslide areas are derived, the SCP, CP, SHP, smoothness, and compactness values were set to 10, 0.9, 0.1, 0.5, and 0.5, respectively, for the implementation of MRS using the eCognition<sup>®</sup> software (Version 9.0.1). Figure 4 shows the segmentation results of the Fanjiaping and Tanjiahe landslides. The study area was segmented into 124,511 objects, including 17,612  $O_{LS}$ . The mapped  $O_{LS}$  covered an area of 4.92 km<sup>2</sup> which represents 12.79% of the study area. The smallest landslide covered an area of 7077 m<sup>2</sup>, whereas the largest, which is the Fanjiaping landslide located on the southern side of the Yangtze River, was 1.5 km<sup>2</sup>.

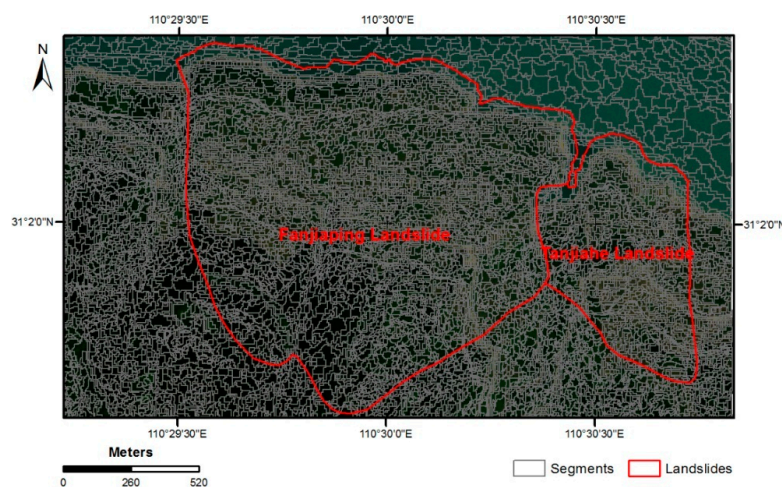


**Figure 4.** True color composite (R: 3, G: 2, B: 1) image overlaid by the segments; colors may not be apparent due to the density of the details: examples of the Fanjiaping and Tanjiahe Landslides.

Based on the varSelRF package, the features used in the final landslide mapping were reduced from 124 to 26. The selected features are shown in Table 3.

**Table 3.** Selected features used in this study.

Features (No.)	Layers
Mean (7)	Pan, Hillshade, Roughness, Blue, Green, NIR, Flow Direction
Min (7)	Pan, Hillshade, Roughness, Blue, Green, NIR, Flow Direction
Max (6)	Hillshade, Roughness, Blue, Green, NIR, Flow Direction
Ratio (4)	Hillshade, Blue, NIR, Flow Direction
Stdv (2)	Roughness, NIR

From Table 3, it is inferred that the *Mean*, *Min*, *Max*, and *Ratio* features play the most important roles in the RF based FS method in this study, which is different from [16]. The *NIR* layer is the most important one which is present in all of the features, followed by *Hillshade*, *Roughness*, *Blue*, and *Flow Direction*, which are all shown in four of the five selected features. Features *Green* and *Pan* were also present three times and twice, respectively.

### 3.2. Landslide Mapping Accuracy Assessment

For quantitative evaluation, the mapped landslides were compared with the landslide reference maps, using seven evaluation indices, i.e., *Completeness*, *Correctness*, *Quality*, *User's accuracy (UA)*, *Producer's accuracy (PA)*, *Overall accuracy (OA)*, and *Kappa coefficient (KAPPA)*.

*Completeness*, *Correctness*, and *Quality* can be expressed by the following equations:

$$\text{Completeness} = A_m / A_{gt} \quad (3)$$

$$\text{Correctness} = A_m / A_e \quad (4)$$

$$\text{Quality} = A_m / (A_e + A_{umgt}) \quad (5)$$

where  $A_m$  is the total area of the mapped landslides that are matched with the ground truth,  $A_{gt}$  is the total area of the ground truth,  $A_e$  is the total area of the mapped landslides, and  $A_{umgt}$  is the total area of the ground truth that are unmatched with the mapped landslides.

In these seven evaluation indices, the higher the index values, the higher the accuracy.

Initially, 20% of the  $O_{LS}$  and  $O_{NLS}$  were randomly selected as training data, and then a 10-fold cross validation method was used, along with the selected feature subset shown in Table 3, to train the RFLM model. Then the test sets were classified using the trained model, and the classification accuracies were  $85.5\% \pm 0.44\%$  (*UA*),  $66.4\% \pm 0.27\%$  (*PA*),  $93.3\% \pm 0.12\%$  (*OA*), and  $71.7\% \pm 0.29\%$  (*KAPPA*), respectively. Then the landslides of the whole study area were mapped using the trained RFLM model, and the result is shown in Figure 5a. In order to improve the performance of the RFLM result, the closing and opening mathematical morphology operations and their combinations were used, corresponding to RFCLM (closing), RFOLM (opening), RFOCLM (opening followed by closing), and RFCOLM (closing followed by opening), respectively. The results are shown in Figure 5b–e. To evaluate the advantages of the mathematical morphology operations, the accuracies obtained after each has been applied are compared with the RFLM. The final quantitative evaluation results are presented in Table 4.

From the point of view of *Completeness* and *PA*, the RFCLM method provides improved results over the other four methods, while the performances of RFLM in these two indices are neither the best nor worst among the five methods. Compared with RFLM, the values of *Completeness* and *PA* of RFOLM and RFOCLM deteriorate to  $63.8\% \pm 0.88\%$ ,  $64.1\% \pm 0.97\%$ ,  $67.8\% \pm 0.89\%$ , and  $67.6\% \pm 0.97\%$ , respectively, while the values of *Completeness* and *PA* of RFCLM and RFCOLM increase to  $84.1\% \pm 0.36\%$ ,  $84.2\% \pm 0.61\%$ ,  $81.5\% \pm 0.47\%$ , and  $83.0\% \pm 0.66\%$ , respectively.

They indicate that the MM closing can improve *Completeness* and *PA*, but the MM opening reduces the two indices.

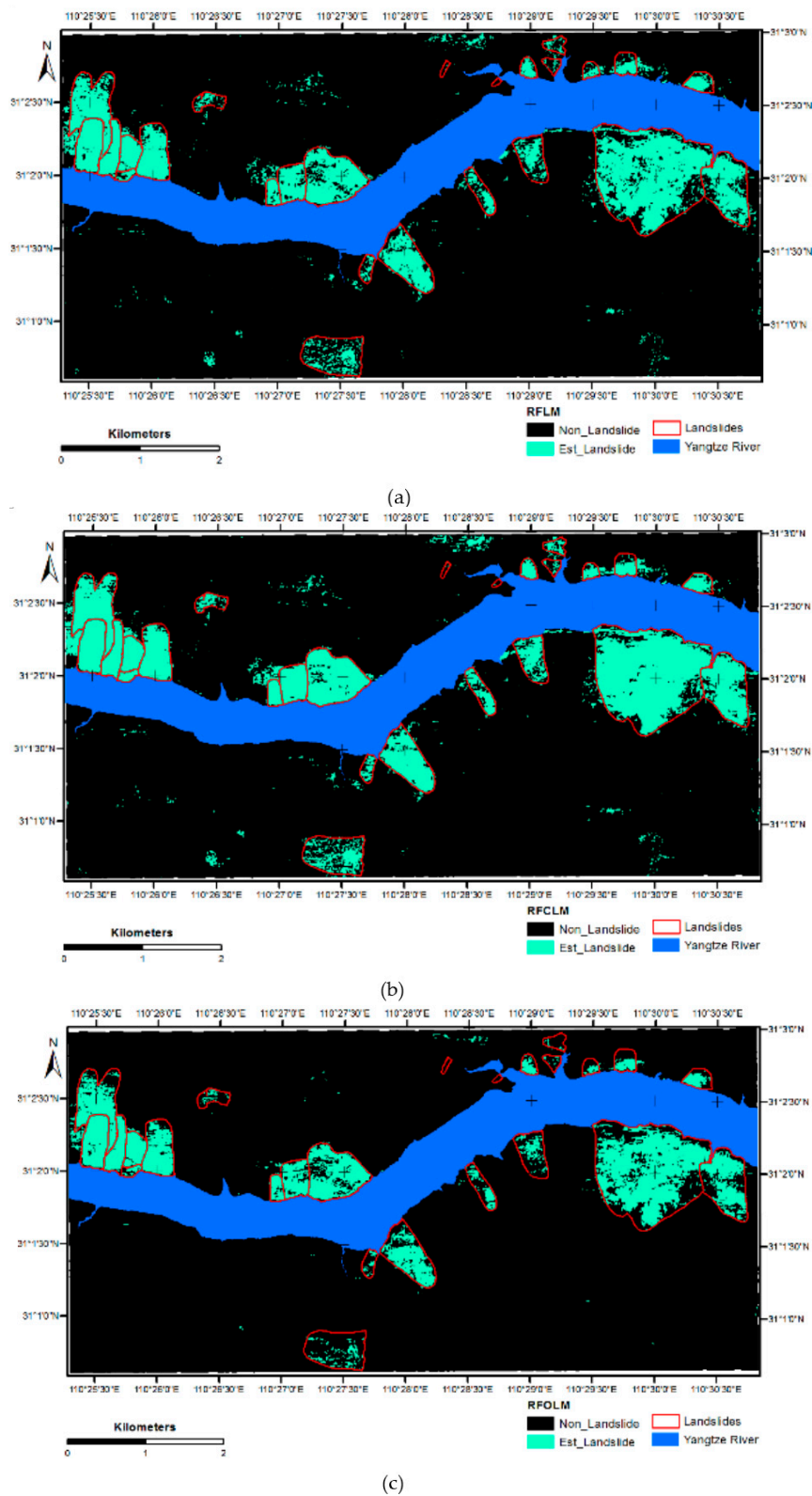
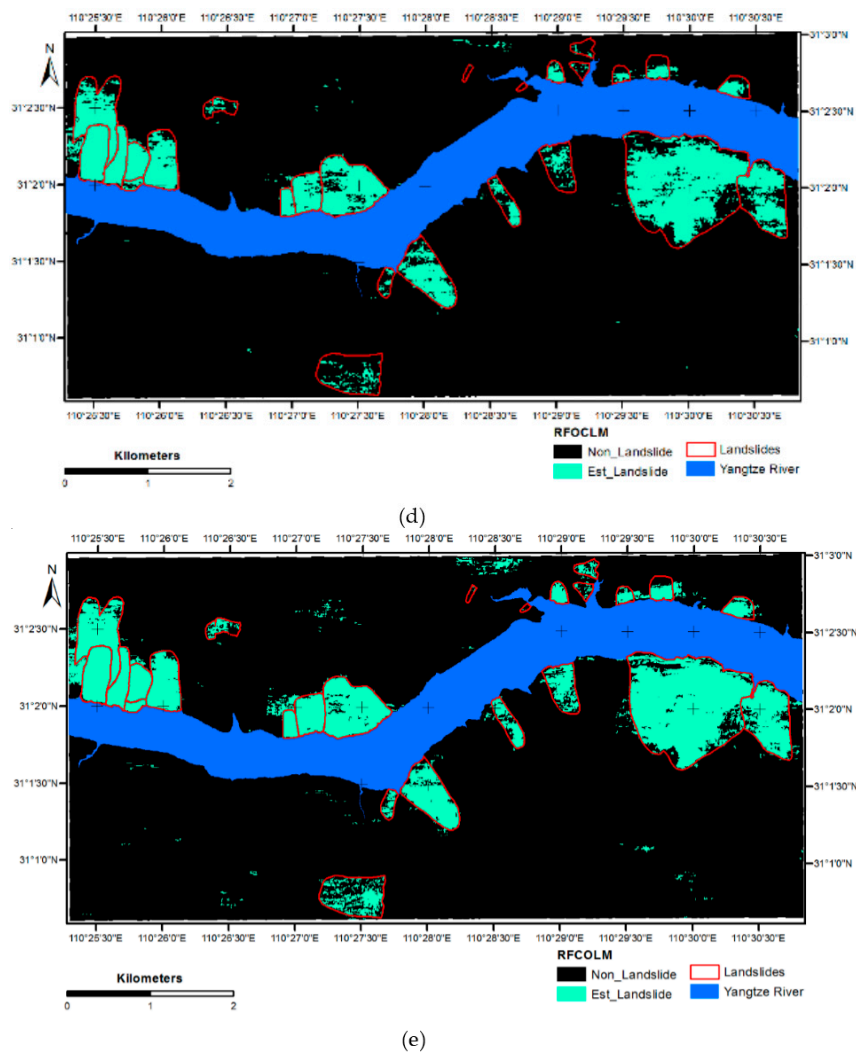


Figure 5. Cont.



**Figure 5.** Landslide mapping results. (a) RFLM. (b) RFCLM. (c) RFOLM. (d) RFOCLM. (e) RFCOLM.

**Table 4.** Quantitative evaluation of the proposed methods in the study area together with the estimated standard deviations (The bolded number means the highest accuracy in each row).

Methods	Completeness (%)	Correctness (%)	Quality (%)	UA (%)	PA (%)	OA (%)	KAPPA (%)
RFLM	71.9 ± 0.13	91.5 ± 0.07	67.1 ± 0.45	89.7 ± 0.44	72.9 ± 0.72	95.0 ± 0.08	77.6 ± 0.43
RFCLM	<b>84.1 ± 0.36</b>	90.9 ± 0.11	77.0 ± 0.48	89.2 ± 0.52	<b>84.2 ± 0.61</b>	96.3 ± 0.09	84.4 ± 0.38
RFOLM	63.8 ± 0.88	<b>97.6 ± 0.13</b>	61.2 ± 0.56	<b>96.9 ± 0.42</b>	64.1 ± 0.97	94.6 ± 0.13	74.3 ± 0.76
RFOCLM	67.8 ± 0.89	<b>97.4 ± 0.12</b>	65.9 ± 0.69	<b>96.9 ± 0.44</b>	67.6 ± 0.97	95.1 ± 0.13	77.0 ± 0.74
RFCOLM	81.5 ± 0.47	93.5 ± 0.08	<b>77.6 ± 0.39</b>	92.8 ± 0.53	83.0 ± 0.66	<b>96.7 ± 0.1</b>	<b>85.7 ± 0.44</b>

Legend for the abbreviations: RFLM: Landslide mapping based on the RF method; RFCLM: Landslide mapping based on the RF method and Closing operation; RFOLM: Landslide mapping based on the RF method and Opening operation; RFOCLM: Landslide mapping based on the RF method and Opening followed by Closing operation; RFCOLM: Landslide mapping based on the RF method and Closing followed by Opening operation.

As for *Correctness* and *UA*, the RFLM provides slightly better results than RFCLM but they are not as good as for the other three models. RFOLM and RFOCLM achieve similar performance, and both obtain the best performance among all models. Values for *Correctness* and *UA* of RFOCLM are almost the same as for RFOLM, which are  $97.4\% \pm 0.12\%$ ,  $96.9\% \pm 0.44\%$ ,  $97.6\% \pm 0.13\%$ , and  $96.9\% \pm 0.42\%$ , respectively. This indicates that regarding the values for *Completeness* and *UA*, MM opening improves *Correctness* and *UA* while MM closing decreases these two evaluation indices.

In terms of *Quality* and *KAPPA*, the best performances for both are obtained by RFCOLM, while RFLM is ranked 3rd of the five methods. MM opening does not improve the *Quality* and *KAPPA* evaluations of RFOLM, because they decrease to  $61.2\% \pm 0.56\%$  and  $74.3\% \pm 0.76\%$ , respectively, compared with the value of RFLM, while MM closing does improve the *Quality* evaluation index, which increases to  $77.0\% \pm 0.48\%$ , and  $77.6\% \pm 0.39\%$ , respectively.

From the perspective of *OA*, it can be seen that the five methods have similar values, with the highest value of  $96.7\% \pm 0.1\%$ , which occurred for the RFCOLM method.

It is known that MM closing can fill holes inside landslide candidates [20], while MM opening is employed to remove errors outside the landslide candidates, so MM closing can increase the  $A_m$ ,  $A_e$ ,  $A_{umgt}$ , and the number of estimate landslide candidates, and MM opening can decrease them. However,  $A_{gt}$  and the number of reference landslides is constant, so MM closing can improve *Completeness*, *PA*, *Quality*, and *KAPPA*, while MM opening causes the opposite effect. MM opening can improve *Correctness* and *UA*, while MM closing causes these two indices to decrease slightly.

Based on the above, it is clear that overall the RFCOLM method has the best performance among these five methods, since it resulted in the three highest accuracies out of the seven evaluation indices, and produced better results than the RFLM method in all evaluation indices. Compared with [36], we have found that *UA*, *PA*, and *OA* are all increased by using the MM operations. Then, we evaluated the statistical significance of the improvement of the landslide mapping results in terms of the accuracies when including the MM operation after RFLM, by using the McNemar's test with a 5% significance level for each pair of the landslide mapping results. According to the calculated  $\chi^2$  and  $z$  values, the null hypothesis ( $H_0$ ) of no significant difference between the two landslide map accuracies is rejected. This means that the use of MM operation is beneficial for RF-based landslide mapping.

#### 4. Discussion

It is significant that the features selected for LM all belong to the layer features (Table 3), while none of the texture or geometry features were selected for the present study, but in [16] the use of texture and geometry features resulted in increases in the landslide mapping accuracy. Since the materials in most of the landslides in this study area are rock and shallow soil, the mechanisms of the landslides result in differences in the spectral information in the surrounding areas. For example, most of the landslides have low NDVI values, while the surrounding areas have high NDVI values. This is because the vegetation cover on the landslides sites has been damaged.

Although the spatial resolution of current satellite images can be as small or less than 1 m, obtaining LM reliably from satellite remote sensing images is still a challenging task. The proposed methods resulted in good performance for LM in the present study by combining the RF algorithm with a mathematical morphology operation. Compared with the similar study area in TGR, the *UA*, *PA*, and *OA* obtained in this study are higher than in [16,43]. The researchers in [16] used airborne LIDAR to map landslides in TGR by using the support vector machine (SVM) and RF method, for which the highest *UA* ( $67.21\% \pm 0.10\%$ ), *PA* ( $71.78\% \pm 0.24\%$ ), and *OA* ( $77.36\% \pm 0.13\%$ ) were obtained. The researchers in [43] used a feature reduced and RF algorithm to map landslides in TGR. They obtained *UA*, *PA*, and *OA* in their research of  $68.45\% \pm 0.05\%$ ,  $72.91\% \pm 0.05\%$ ,  $78.24\% \pm 0.03\%$ , respectively, while this study revealed a *UA* of  $92.8\% \pm 0.53\%$ , *PA* of  $83.0\% \pm 0.66\%$ , and *OA* of  $96.7\% \pm 0.1\%$ .

However, some uncertainties still remain. First of all, the segmentation process can introduce uncertainties in LM, because the landslide reference cannot be segmented into exact objects. Although some segmentation methods are available in eCognition® (Version 9.0.1), errors are inevitable, which will decrease the accuracy of LM [43]. Second, there are several key parameters in the RF based LM methods that need to be adjusted for different experiments. Generally speaking, applying different parameter values may improve or worsen the final results. Thus, a trial-and-error optimization method may be the most effective way to find the optimal parameter values in practical applications. Third,

since the proposed model did not work well for slow-moving landslides which exist in TGR, this will be the research focus in the future.

## 5. Conclusions

This paper has applied a hybrid model within the framework of object-oriented landslide mapping to identify landslides in the Three Gorges Reservoir area from 'ZY-3' high spatial resolution satellite images. The proposed model utilizes the greater generalization capabilities of RFs for the effective elimination of redundant features by a feature selection method together with mathematical morphology operations.

Three object-feature domains, which contain 124 features, were generated from the 'ZY-3' HSR satellite data. By using the feature selection method based on the RF algorithm, 26 features were selected for the feature subset. Since most of the selected features were derived from the image layers, it can be concluded that the multi-spectral band 'ZY-3' HSR satellite image provides adequate information and therefore the proposed feature selection method can provide effective information for landslide mapping in the TGR area.

Training sets which consisted of 20% of  $O_{LS}$  and  $O_{NLS}$  were used to train the RF model based on the selected feature subsets, and  $UA$ ,  $PA$ ,  $OA$ , and  $KAPPA$  of the RFLM for the remaining test sets were found to be  $85.5\% \pm 0.44\%$  ( $UA$ ),  $66.4\% \pm 0.27\%$  ( $PA$ ),  $93.3\% \pm 0.12\%$  ( $OA$ ), and  $71.7\% \pm 0.29\%$  ( $KAPPA$ ). Four different mathematical morphology operations based on closing and opening and their combinations, were used to improve the performance of the RFLM. Besides  $UA$ ,  $PA$ ,  $OA$ , and  $KAPPA$ , another three evaluation indices were used to compare the performance of these five LM models. Overall, the RFCOLM method has the best performance among the five LM methods. The results showed that MM operations can clearly improve the performance of RFLM in each accuracy evaluation index. Thus, it can be concluded that, by using the features extracted from 'ZY-3' HSR satellite data, the feature selection method, a random forests algorithm and MM method, provides an effective method for object-oriented landslide identification in the TGR.

**Acknowledgments:** This work was supported in part by the National Natural Science Foundation of China (61601418); and in part by the National High Technology Research and Development Program of China (2012AA121303). The authors would like to thank the handling editor and anonymous reviewers for their valuable comments and suggestions, which significantly improved the quality of this paper.

**Author Contributions:** Tao Chen implemented all the landslide mapping methods in the eCognition® and R statistical programming environment, conducted the experiments, and finished the first draft. John C. Trinder and Ruiqing Niu supervised the research, and John C. Trinder contributed to the editing and review of the manuscript.

**Conflicts of Interest:** The authors declare no conflict of interest.

## References

1. Liu, C.Z.; Liu, Y.H.; Wen, M.S.; Li, T.F.; Lian, J.F.; Qin, S.W. Geo-Hazard Initiation and Assessment in the Three Gorges Reservoir. In *Landslide Disaster Mitigation in Three Gorges Reservoir, China*; Wang, F.W., Li, T.L., Eds.; Springer: Berlin/Heidelberg, Germany, 2009; pp. 3–40.
2. Keefer, D.K.; Larsen, M.C. Assessing landslide hazards. *Science* **2007**, *316*, 1136–1138. [[CrossRef](#)] [[PubMed](#)]
3. Huang, R.; Fan, X. The landslide story. *Nat. Geosci.* **2013**, *6*, 325–326. [[CrossRef](#)]
4. Niu, R.; Wu, X.; Yao, D.; Peng, L.; Ai, L.; Peng, J. Susceptibility assessment of landslides triggered by the Lushan earthquake, April 20, 2013, China. *IEEE J. Sel. Top. Appl. Earth Obs. Remote Sens.* **2014**, *7*, 3979–3992. [[CrossRef](#)]
5. Keefer, J. Landslide risks rise up agenda. *Nature* **2014**, *511*, 272–273.
6. Nagarajan, R.; Mukherjee, A.; Roy, A.; Khire, M. Technical note temporal remote sensing data and GIS application in landslide hazard zonation of part of Western Ghat, India. *Int. J. Remote Sens.* **1998**, *19*, 573–585. [[CrossRef](#)]
7. Van Westen, C.J.; Castellanos, E.; Kuriakose, S.L. Spatial data for landslide susceptibility, hazard, and vulnerability assessment: An overview. *Eng. Geol.* **2008**, *102*, 112–131. [[CrossRef](#)]

8. Stumpf, A.; Kerle, N. Object-oriented mapping of landslides using Random Forests. *Remote Sens. Environ.* **2011**, *115*, 2564–2577. [[CrossRef](#)]
9. Scaioni, M.; Longoni, L.; Melillo, V.; Papini, M. Remote sensing for landslide investigations: An overview of recent achievements and perspectives. *Remote Sens.* **2014**, *6*, 9600–9652. [[CrossRef](#)]
10. Galli, M.; Ardizzone, F.; Cardinali, M.; Guzzetti, F.; Reichenbach, P. Comparing landslide inventory maps. *Geomorphology* **2008**, *94*, 268–289. [[CrossRef](#)]
11. Metternicht, G.; Hurni, L.; Gogu, R. Remote sensing of landslides: An analysis of the potential contribution to geo-spatial systems for hazard assessment in mountainous environments. *Remote Sens. Environ.* **2005**, *98*, 284–303. [[CrossRef](#)]
12. Guzzetti, F.; Mondini, A.C.; Cardinali, M.; Fiorucci, F.; Santangelo, M.; Chang, K.T. Landslide inventory maps: New tools for an old problem. *Earth Sci. Rev.* **2012**, *112*, 42–66. [[CrossRef](#)]
13. Hervas, J.; Barredo, J.I.; Rosin, P.L.; Pasuto, A.; Mantovani, F.; Silvano, S. Monitoring landslides from optical remotely sensed imagery: The case history of Tessina landslide, Italy. *Geomorphology* **2003**, *54*, 63–75. [[CrossRef](#)]
14. Kieffer, D.S.; Jibson, R.; Rathje, E.M.; Kelson, K. Landslides triggered by the 2004 Niigata Ken Chuetsu, Japan, earthquake. *Earthq. Spectra* **2006**, *22*, 47–73. [[CrossRef](#)]
15. Voigt, S.; Kemper, T.; Riedlinger, T.; Kie, R.; Scholte, K.; Mehl, H. Satellite image analysis for disaster and crisis-management support. *IEEE Trans. Geosci. Remote Sens.* **2007**, *45*, 1520–1528. [[CrossRef](#)]
16. Chen, W.; Li, X.; Wang, Y.; Chen, G.; Liu, S. Forested landslide detection using LiDAR data and the random forest algorithm: A case study of the Three Gorges, China. *Remote Sens. Environ.* **2014**, *152*, 291–301. [[CrossRef](#)]
17. Hilley, G.E.; Burgmann, R.; Ferretti, A.; Novali, F.; Rocca, F. Dynamics of slow-moving landslides from permanent scatterer analysis. *Science* **2004**, *304*, 1952–1955. [[CrossRef](#)] [[PubMed](#)]
18. Lu, P.; Casagli, N.; Catani, F.; Tofani, V. Persistent Scatterers Interferometry Hotspot and Cluster analysis (PSI-HCA) for detection of extremely slow-moving landslides. *Int. J. Remote Sens.* **2012**, *33*, 466–489. [[CrossRef](#)]
19. Lu, D.; Mausel, P.; Brondizio, E.; Moran, E. Change detection techniques. *Int. J. Remote Sens.* **2004**, *25*, 2365–2401. [[CrossRef](#)]
20. Li, Z.; Shi, W.; Myint, S.W.; Lu, P.; Wang, Q. Semi-automated landslide inventory mapping from bitemporal aerial photographs using change detection and level set method. *Remote Sens. Environ.* **2016**, *175*, 215–230. [[CrossRef](#)]
21. Travelletti, J.; Malet, J.P.; Delacourt, C. Image-based correlation of Laser Scanning point cloud time series for landslide monitoring. *Int. J. Appl. Earth Obs.* **2014**, *32*, 1–18. [[CrossRef](#)]
22. Cheng, G.; Guo, L.; Zhao, T.; Han, J.; Li, H.; Fang, J. Automatic landslide detection from remote-sensing imagery using a scene classification method based on BoVW and pLSA. *Int. J. Remote Sens.* **2013**, *34*, 45–59. [[CrossRef](#)]
23. Moosavi, V.; Talebi, A.; Shirmohammadi, B. Producing a landslide inventory map using pixel-based and object-oriented approaches optimized by Taguchi method. *Geomorphology* **2014**, *204*, 646–656. [[CrossRef](#)]
24. Blaschke, T. Object based image analysis for remote sensing. *ISPRS-J. Photogramm. Remote Sens.* **2010**, *65*, 2–16. [[CrossRef](#)]
25. Lu, P.; Stumpf, A.; Kerle, N.; Casagli, N. Object-oriented change detection for landslide rapid mapping. *IEEE Geosci. Remote Sens. Lett.* **2011**, *8*, 701–705. [[CrossRef](#)]
26. Martha, T.R.; Kerle, N.; van Westen, C.J.; Jetten, V.; Kumar, K.V. Segment optimization and data-driven thresholding for knowledge-based landslide detection by object-based image analysis. *IEEE Trans. Geosci. Remote Sens.* **2011**, *49*, 4928–4943. [[CrossRef](#)]
27. Behling, R.; Roessner, S.; Kaufmann, H.; Kleinschmit, B. Automated spatiotemporal landslide mapping over large areas using rapideye time series data. *Remote Sens.* **2014**, *6*, 8026–8055. [[CrossRef](#)]
28. Behling, R.; Roessner, S.; Golovko, D.; Kleinschmit, B. Derivation of long-term spatiotemporal landslide activity—A multi-sensor time series approach. *Remote Sens. Environ.* **2016**, *186*, 88–104. [[CrossRef](#)]
29. Pradhan, B.; Jebur, M.N.; Shafri, H.Z.M.; Tehrani, M.S. Data Fusion Technique Using Wavelet Transform and Taguchi Methods for Automatic Landslide Detection From Airborne Laser Scanning Data and QuickBird Satellite Imagery. *IEEE Trans. Geosci. Remote Sens.* **2016**, *54*, 1610–1622. [[CrossRef](#)]
30. Breiman, L. Random Forests. *Mach. Learn.* **2001**, *45*, 5–32. [[CrossRef](#)]
31. Lawrence, R.L.; Wood, S.D.; Sheley, R.L. Mapping invasive plants using hyperspectral imagery and Breiman Cutler classifications (randomForest). *Remote Sens. Environ.* **2006**, *100*, 356–362. [[CrossRef](#)]

32. Stumpf, A.; Lachiche, N.; Malet, J.P.; Kerle, N.; Puissant, A. Active learning in the spatial domain for remote sensing image classification. *IEEE Trans. Geosci. Remote Sens.* **2014**, *52*, 2492–2507. [[CrossRef](#)]
33. Soille, P. *Morphological Image Analysis: Principles and Applications*; Springer: New York, NY, USA, 2003.
34. Liu, J.G.; Mason, P.J.; Clerici, N.; Chen, S.; Davis, A.; Miao, F.; Deng, H.; Liang, L. Landslide hazard assessment in the Three Gorges area of the Yangtze river using ASTER imagery: Zigui-Badong. *Geomorphology* **2004**, *61*, 171–187. [[CrossRef](#)]
35. Duro, D.C.; Franklin, S.E.; Dube, M.G. Multi-scale object-based image analysis and feature selection of multi-sensor earth observation imagery using random forests. *Int. J. Remote Sens.* **2012**, *33*, 4502–4526. [[CrossRef](#)]
36. Baatz, M.; Schäpe, A. Multiresolution segmentation: An optimization approach for high quality multi-scale image segmentation. Available online: [http://www.ecognition.com/sites/default/files/405\\_baatz\\_fp\\_12.pdf](http://www.ecognition.com/sites/default/files/405_baatz_fp_12.pdf) (accessed on 9 January 2017).
37. Definiens Professional Earth (DPE). *Definiens Professional 5 User Guide*; Definiens AG: München, Germany, 2006; p. 249.
38. Martha, T.R.; Kerle, N.; van Westen, C.J.; Kumar, K.V. Characterising spectral, spatial and morphometric properties of landslides for semi-automatic detection using object-oriented methods. *Geomorphology* **2010**, *116*, 24–36. [[CrossRef](#)]
39. Haralick, R.M.; Shanmugam, K.; Dinstein, I.H. Textural features for image classification. *IEEE Trans. Syst. Man Cybern.* **1973**, *SMC-3*, 610–621. [[CrossRef](#)]
40. Laliberte, A.S.; Rango, A. Texture and scale in object-based analysis of subdecimeter resolution unmanned aerial vehicle (UAV) imagery. *IEEE Trans. Geosci. Remote Sens.* **2009**, *47*, 761–770. [[CrossRef](#)]
41. Trimble. *eCognition Developer 8.64.0 Reference Book*; Trimble Documentation; Trimble Germany GmbH: Munich, Germany, 2011.
42. Cutler, D.R., Jr.; Edwards, T.C.; Beard, K.H.; Cutler, A.; Hess, K.T. Random forests for classification in ecology. *Ecology* **2007**, *88*, 2783–2792. [[CrossRef](#)] [[PubMed](#)]
43. Li, X.; Cheng, X.; Chen, W.; Chen, G.; Liu, S. Identification of forested landslides using LiDAR data, object-based image analysis, and machine learning algorithms. *Remote Sens.* **2015**, *7*, 9705–9726. [[CrossRef](#)]
44. Kursu, M.B.; Rudnicki, W.R. Feature selection with the Boruta package. *J. Stat. Softw.* **2010**, *36*, 1–13. [[CrossRef](#)]
45. Kohavi, R.; John, G.H. Wrappers for feature subset selection. *Artif. Intell.* **1997**, *97*, 273–324. [[CrossRef](#)]
46. Diaz-Uriarte, R. varSelRF. Available online: <https://cran.r-project.org/web/packages/varSelRF/varSelRF.pdf> (accessed on 9 January 2017).
47. R Development Core Team. *R: A Language and Environment for Statistical Computing*; R Foundation for Statistical Computing: Vienna, Austria, 2006.
48. Liaw, A. RandomForest: Breiman and Cutler’s Random Forests for Classification and Regression. Version 4.6-12. 2015. Available online: <https://cran.r-project.org/web/packages/randomForest/randomForest.pdf> (accessed on 9 January 2017).
49. Diaz-Uriarte, R.; Alvarez de Andres, S. Gene selection and classification of microarray data using random forest. *BMC Bioinform.* **2006**. [[CrossRef](#)] [[PubMed](#)]
50. Dragut, L.; Csillik, O.; Eisank, C.; Tiede, D. Automated parameterisation for multi-scale image segmentation on multiple layers. *ISPRS J. Photogramm. Remote Sens.* **2014**, *88*, 119–127. [[CrossRef](#)] [[PubMed](#)]
51. Myint, S.W.; Gober, P.; Brazel, A.; Grossman-Clarke, S.; Weng, Q. Per-pixel vs. object-based classification of urban land cover extraction using high spatial resolution imagery. *Remote Sens. Environ.* **2011**, *115*, 1145–1161. [[CrossRef](#)]
52. Aksoy, B.; Ercanoglu, M. Landslide identification and classification by object-based image analysis and fuzzy logic: An example from the Azdavay region (Kastamonu, Turkey). *Comput. Geosci.* **2012**, *38*, 87–98. [[CrossRef](#)]

